

Supporting Information

for

**Intrinsic microkinetic effects of spray-drying and SiC co-support on
Mn-Na₂WO₄/SiO₂ catalysts used in oxidative coupling of methane**

Gontzal Lezcano,^a Shekhar R. Kulkarni,^a Vijay K. Velisoju,^a Natalia Realpe,^a Pedro Castaño^{a,b*}

^a Multiscale Reaction Engineering, KAUST Catalysis Center (KCC), King Abdullah University of Science and Technology, Thuwal 23955-6900, Saudi Arabia

^b Chemical Engineering Program, Physical Science and Engineering (PSE) Division, King Abdullah University of Science and Technology

*Corresponding author: pedro.castano@kaust.edu.sa

S1. Homogeneous kinetic model

Having a reliable gas-phase mechanism is of utmost importance for the accurate microkinetic modeling of OCM reactions. OCM is a complex process involving simultaneous reactions in the gas phase and on the catalytic surface. However, using mechanisms with hundreds of reactions and species can present challenges and cause inconvenience, since considerable computational resources and time would be required for simulations. In this context, Wang et al.¹ conducted a comprehensive investigation into the most reliable gas-phase frameworks for catalyst-free OCM. They compared their experimental results obtained under methane-rich operating conditions in a jet-stirred reactor with the results of nine existing gas-phase network models. The observed trends under various operating conditions for OCM were successfully captured by very detailed combustion models such as AramcoMech 3.0,² CRECK,³ NUIGMech1.1,⁴ GRI-Mech 3.0⁵ and USC Mech II.⁶ By contrast, models originally derived from catalytic processes exhibited poor agreement with the experimental trends. While it is preferable to have very detailed gas-phase models for describing the most accurate kinetics, a large number of gas-phase species significantly increases the number of equations in the 1D heterogeneous model. This is because gas-phase species appear at each collocation point of both interstitial and interparticle phase mass balances. In fact, the number of species and reactions in the models ranges from 53 and 325 (GRI-Mech 3.0) to 2746 and 11,270 (NUIGMech1.1). Furthermore, most microkinetic models for OCM with a catalyst either have *ad-hoc* gas-phase models or have reduced versions of full-range models. Considering these factors, this study used a homogeneous kinetic model that accounts for gas-phase reactions in OCM while prioritizing the associated computational complexity.

The first group of *ad-hoc* gas-phase mechanisms developed for OCM consists of models with a large number of reactions (>100). For instance, Simon et al.,⁷ Fleys et al.,⁸ and Simon and Marquaire⁹ employed a gas-phase reaction network comprising over 450 elementary reactions for their OCM experiments with a lanthanum oxide catalyst in a jet-stirred reactor, which included 19 surface reactions. Their gas-phase model encompasses all elementary reactions involving molecules and radicals containing fewer than three carbon

atoms. This model was validated using a significant amount of experimental data.¹⁰ Similarly, Mims et al.¹¹ developed a homogeneous model for OCM with almost 450 reversible elementary gas-phase reactions involving 115 species on the basis of isotopic studies with a Li/MgO catalyst. Zanthoff and Baerns¹² constructed their reaction scheme with 164 reaction steps and 28 species on the basis of kinetic values reported in the literature and then validated the scheme by conducting OCM experiments without a catalyst. According to their gas-phase kinetics, excess methane leads to high C₂ concentrations and thereby promotes the formation of oxygen-containing radicals. They deduced that the C₂ selectivity to CH₃• radical concentration via the coupling reaction and thus, a high concentration of the latter is fundamental for enhanced C₂ selectivities. Similarly, Geerts et al.¹³ modeled OCM reactions in the gas phase in the presence and absence of a catalyst (Li/MgO) by assuming a PFR and developed a gas-phase mechanism by reducing their original mechanism of 400 reactions to 164 by, among other methods, ignoring CH₃OH formation routes; their model was constructed by considering key reactive species that they identified, such as H•, OH•, HO₂•, and CH₃•.

Chen et al. took a major stride toward reducing gas-phase reaction mechanisms for OCM.¹⁴ They began with the models of Zanthoff and Baerns¹² and Geerts et al.¹³ and managed to reduce the reaction mechanisms to 66 reactions and 20 species. This reduction involved disregarding certain species, such as CH₃CHO, which was deemed to be insignificant in stoichiometric methane-air flames. Consequently, intermediates such as the CH₃CO• radical were also excluded. Additionally, the use of high temperatures in OCM experiments allowed the exclusion of CH₃OOH, which becomes significant in degenerate branching during methane oxidation at low temperatures (around 400 °C). Notable species that were omitted included CH₃OH, CH• radical, and CH₂• radical. Through their experiments in the absence of a catalyst and by using sensitivity analyses and contribution analyses, Chen et al.¹⁴ further refined their model to 33 reactions by ignoring most of the reactions involving H₂-O₂ mixtures and species such as H•, O•, OH•, and HO₂•, with minimal impact on model performance. In a subsequent study, Chen et al.¹⁵ extended their reduced model by incorporating the effect of co-feeding C₂H₆ in the presence and absence of a catalyst (Li/MgO), and the

resulting model involved 39 reactions. They validated their model at $P = 100\text{--}400$ kPa, $T = 973\text{--}1083$ K, and feed ratios of $\text{CH}_4/\text{O}_2 = 4\text{--}5$ and $\text{C}_2\text{H}_6/\text{CH}_4 = 0\text{--}0.1$. In the absence of a catalyst, they observed that co-feeding ethane significantly enhanced OCM conversions owing to the presence of $\text{C}_2\text{H}_5^\bullet$ radicals and the increased abundance of CH_3^\bullet and HO_2^\bullet radicals; all these radicals were attributed to the weaker C–H bond in ethane. The more pronounced increase in the concentration of the HO_2^\bullet radical was used to explain the decrease in C_2 selectivity in absence of a catalyst. The model was also validated for a total pressure range of $P = 100\text{--}1000$ kPa by including the falloff pressure effect for three-body reactions.¹⁶

In the present work, the model of Chen et al.¹⁵ with 39 reactions and 23 gas-phase species was selected for use. The set of 39 homogeneous reversible elementary reactions are presented in Table S1.

It should be noted that while the incorporation of reduced homogeneous mechanisms specifically developed for OCM, such as the mechanism proposed by Chen et al.,¹⁵ may result in a reduction of the predictive capabilities of the model in the absence of a catalyst, it offers a favorable trade-off between simplicity and accuracy in representing the role of gas-phase kinetics under catalytic OCM conditions. In this context, despite acknowledging the limitations of Chen et al.'s model,¹⁵ Karakaya et al.^{17,18} still opted to use it because of its simplicity; they adjusted certain prefactor values to match their spatially resolved concentration and temperature profiles. Similarly, Reyes et al.¹⁹ coupled homogeneous reactions with a pellet-scale catalytic model by using the model of Zanthoff and Baerns.¹² However, Chen et al.'s model¹⁵ is the most extensively used model in the literature to account for gas-phase contributions for a wide array of OCM catalyst families, including Li/MgO, La-Sr/CaO, Sr/La₂O₃, and Mn-Na₂WO₄/SiO₂.^{20–29} Other authors have adapted larger mechanisms to suit their specific applications. For example, Vandewalle et al.³⁰ used a reduced version of AramcoMech 1.3,³¹ which consisted of 317 reactions involving 57 species.

Table S1. Set of homogeneous reversible elementary reactions reported by Chen et al.¹⁵ and used in the present work, along with the forward rate parameters. Units: A_j^f (order 1) s^{-1} , A_j^f (order 2) $kmol^{-1} m_g^3 s^{-1}$, A_j^f (order 3) $kmol^{-2} m_g^6 s^{-1}$, $E_{a,j}^f$ $kJ mol^{-1}$.

Step	Equation	A_j^f	$E_{a,j}^f$
1	$CH_4(g) + O_2(g) \rightleftharpoons CH_3^{\cdot}(g) + HO_2^{\cdot}(g)$	$9.83 \cdot 10^9$	193.86
2	$CH_4(g) + H^{\cdot}(g) \rightleftharpoons CH_3^{\cdot}(g) + H_2(g)$	$2.34 \cdot 10^{11}$	51.17
3	$CH_4(g) + O^{\cdot}(g) \rightleftharpoons CH_3^{\cdot}(g) + OH^{\cdot}(g)$	$1.27 \cdot 10^{12}$	33.83
4	$CH_4(g) + OH^{\cdot}(g) \rightleftharpoons CH_3^{\cdot}(g) + H_2O(g)$	$7.43 \cdot 10^{11}$	41.43
5	$CH_4(g) + HO_2^{\cdot}(g) \rightleftharpoons CH_3^{\cdot}(g) + H_2O_2(g)$	$4.01 \cdot 10^{10}$	99.61
6	$CH_3^{\cdot}(g) + O_2(g) \rightleftharpoons CH_3O^{\cdot}(g) + O^{\cdot}(g)$	$3.08 \cdot 10^{11}$	141.00
7	$CH_3^{\cdot}(g) + O_2(g) \rightleftharpoons CH_2O(g) + OH^{\cdot}(g)$	$4.59 \cdot 10^{10}$	103.66
8	$CH_3^{\cdot}(g) + HO_2^{\cdot}(g) \rightleftharpoons CH_3O^{\cdot}(g) + OH^{\cdot}(g)$	$8.85 \cdot 10^{10}$	0.00
9	$CH_3^{\cdot}(g) + CH_3^{\cdot}(g) + M(g) \rightleftharpoons C_2H_6(g) + M(g)$	$6.50 \cdot 10^{13}$	0.00
10	$CH_3O^{\cdot}(g) + M(g) \rightleftharpoons CH_2O(g) + H^{\cdot}(g) + M(g)$	$2.58 \cdot 10^{17}$	116.00
11	$CH_2O(g) + OH^{\cdot}(g) \rightleftharpoons CHO^{\cdot}(g) + H_2O(g)$	$6.80 \cdot 10^{11}$	6.00
12	$CH_2O(g) + HO_2^{\cdot}(g) \rightleftharpoons CHO^{\cdot}(g) + H_2O_2(g)$	$4.17 \cdot 10^9$	40.12
13	$CH_2O(g) + CH_3^{\cdot}(g) \rightleftharpoons CHO^{\cdot}(g) + CH_4(g)$	$7.00 \cdot 10^{10}$	26.03
14	$CHO^{\cdot}(g) + M(g) \rightleftharpoons CO(g) + H^{\cdot}(g) + M(g)$	$2.80 \cdot 10^{12}$	64.36
15	$CHO^{\cdot}(g) + O_2(g) \rightleftharpoons CO(g) + HO_2^{\cdot}(g)$	$1.71 \cdot 10^8$	0.00
16	$CO(g) + HO_2^{\cdot}(g) \rightleftharpoons CO_2(g) + OH^{\cdot}(g)$	$3.08 \cdot 10^{11}$	107.34
17	$C_2H_6(g) + H^{\cdot}(g) \rightleftharpoons C_2H_5^{\cdot}(g) + H_2(g)$	$9.10 \cdot 10^{11}$	51.70
18	$C_2H_6(g) + OH^{\cdot}(g) \rightleftharpoons C_2H_5^{\cdot}(g) + H_2O(g)$	$6.45 \cdot 10^{11}$	17.16
19	$C_2H_6(g) + CH_3^{\cdot}(g) \rightleftharpoons C_2H_5^{\cdot}(g) + CH_4(g)$	$2.39 \cdot 10^{10}$	64.73
20	$C_2H_5^{\cdot}(g) + HO_2^{\cdot}(g) \rightleftharpoons CH_3^{\cdot}(g) + CH_2O(g) + OH^{\cdot}(g)$	$9.48 \cdot 10^9$	0.00
21	$C_2H_5^{\cdot}(g) + M(g) \rightleftharpoons C_2H_4(g) + H^{\cdot}(g) + M(g)$	$6.96 \cdot 10^{16}$	167.66
22	$C_2H_5^{\cdot}(g) + O_2(g) \rightleftharpoons C_2H_4(g) + HO_2^{\cdot}(g)$	$6.35 \cdot 10^9$	53.20
23	$C_2H_4(g) + O_2(g) \rightleftharpoons C_2H_3^{\cdot}(g) + HO_2^{\cdot}(g)$	$2.81 \cdot 10^9$	144.55
24	$C_2H_4(g) + H^{\cdot}(g) \rightleftharpoons C_2H_3^{\cdot}(g) + H_2(g)$	$1.50 \cdot 10^{11}$	42.7
25	$C_2H_4(g) + OH^{\cdot}(g) \rightleftharpoons C_2H_3^{\cdot}(g) + H_2O(g)$	$6.12 \cdot 10^{10}$	24.7
26	$C_2H_4(g) + CH_3^{\cdot}(g) \rightleftharpoons C_2H_3^{\cdot}(g) + CH_4(g)$	$1.99 \cdot 10^8$	51.46
27	$C_2H_4(g) + OH^{\cdot}(g) \rightleftharpoons CH_3^{\cdot}(g) + CH_2O(g)$	$2.72 \cdot 10^9$	0.00
28	$C_2H_3^{\cdot}(g) + M(g) \rightleftharpoons C_2H_2(g) + H^{\cdot}(g) + M(g)$	$1.21 \cdot 10^{18}$	176.44
29	$C_2H_3^{\cdot}(g) + O_2(g) \rightleftharpoons C_2H_2(g) + HO_2^{\cdot}(g)$	$6.00 \cdot 10^9$	0.00
30	$C_2H_3^{\cdot}(g) + O_2(g) \rightleftharpoons CH_2O(g) + CHO^{\cdot}(g)$	$6.50 \cdot 10^9$	0.00
31	$C_2H_5^{\cdot}(g) + CH_3^{\cdot}(g) \rightleftharpoons C_3H_8(g)$	$8.00 \cdot 10^9$	0.00
32	$C_3H_8(g) + H^{\cdot}(g) \rightleftharpoons C_3H_7^{\cdot}(g) + H_2(g)$	$9.00 \cdot 10^{11}$	32.00
33	$C_2H_4(g) + CH_3^{\cdot}(g) \rightleftharpoons C_3H_7^{\cdot}(g) + CH_4(g)$	$3.00 \cdot 10^8$	29.00
34	$C_3H_7^{\cdot}(g) \rightleftharpoons C_3H_6(g) + H^{\cdot}(g)$	$1.50 \cdot 10^{15}$	156.00
35	$O_2(g) + H^{\cdot}(g) \rightleftharpoons OH^{\cdot}(g) + O^{\cdot}(g)$	$2.20 \cdot 10^{11}$	70.30
36	$O_2(g) + H^{\cdot}(g) + M(g) \rightleftharpoons HO_2^{\cdot}(g) + M(g)$	$1.39 \cdot 10^{11}$	0.00
37	$HO_2^{\cdot}(g) + HO_2^{\cdot}(g) \rightleftharpoons O_2(g) + OH^{\cdot}(g) + OH^{\cdot}(g)$	$2.00 \cdot 10^9$	0.00
38	$H_2O_2(g) + M(g) \rightleftharpoons OH^{\cdot}(g) + OH^{\cdot}(g) + M(g)$	$1.27 \cdot 10^{14}$	199.36
39	$C_2H_6(g) \rightleftharpoons C_2H_5^{\cdot}(g) + H^{\cdot}(g)$	$4.00 \cdot 10^{16}$	378.51

The primary initiation step in Chen et al.'s mechanism¹⁵ (Step 1 in Table S1), which involves the reaction between CH₄ and O₂, is not the main source of CH₃• radicals. Rather, the primary source of CH₃• radicals is H abstraction reactions involving CH₄ and a radical (Steps 2–5 in Table S1), especially the reaction between CH₄ and OH•. Consequently, the generation of OH• from H₂O₂ (Step 38 in Table S1) plays a crucial role in the degenerate branched-chain mechanism, as the majority of OH• radicals are formed through this step; thus, it is a secondary initiation step. Therefore, OH•, and not O•, is the main chain carrier in the proposed mechanism. H₂O₂ produced from the reactions between CH₄ and HO₂• serves as the primary source of OH• radicals, with HO₂• being mainly formed in Steps 15 and 22 in Table S1 from the reaction of O₂ with CHO• and C₂H₅•, respectively. This highlights the significance of these reactions in providing the necessary OH• radicals for the overall mechanism.

The degeneration of the branched chain is primarily caused by the CH₃• radical coupling reaction (Step 9 in Table S1), which acts as the dominant termination step. However, the CH₃• radicals are also heavily consumed in their oxidation chains (Steps 10–16 in Table S1), resulting in the inevitable formation of CH₂O, primarily through the conversion of CH₃O• but also directly from the CH₃• radical. The CH₂O formed can undergo further oxidation to CHO• through its reaction with a CH₃• radical, leading to termination as either CO or further oxidation to CO₂.

The coupling of CH₃• radicals with C₂H₆ is the primary pathway for the formation of C₂ products, while the direct coupling of CH₃• radicals with C₂H₆ is negligible. The production of C₂H₄ is achieved through H abstractions from C₂H₆ (Steps 17–19 and 39 in Table S1) and subsequent (oxo)dehydrogenation of the resulting C₂H₅• radical (Steps 20–22 in Table S1). These routes are in agreement with several works^{12,21,32} that discarded the significant contribution of direct routes to form C₂H₄. C₂H₅• radicals are predominantly formed from C₂H₆ through hydrogen abstractions by various radicals, including H•, OH•, HO₂•, and CH₃•. It is noteworthy that the formation of C₂H₄ from C₂H₆ occurs at higher rates via the pyrolytic chain compared with the oxidative route.¹⁴ Both direct and indirect scission (via HO₂•) of the C-C bond in C₂H₆ are not considered significant because of their higher dissociation energy, especially in comparison with H

abstraction from C_2H_6 by a radical to produce $C_2H_5^{\bullet}$ radicals. Therefore, their contribution to CH_2O formation is negligible in comparison to the amounts produced from CH_3^{\bullet} radicals. C_2H_4 can undergo further reactions, including H abstraction by radicals to form a $C_2H_3^{\bullet}$ radical (Steps 23–26 in Table S1), or it could react with OH^{\bullet} to break the C-C bond (Step 27 in Table S1). C_2H_2 is produced from pyrolytic or oxidative reactions of $C_2H_3^{\bullet}$ radicals (Steps 28 and 29 in Table S1). However, $C_2H_3^{\bullet}$ radicals can also undergo cracking to yield CH_2O and a CH_3O^{\bullet} radical (Step 30 in Table S1). The model also considers the coupling of $C_2H_5^{\bullet}$ and CH_3^{\bullet} radicals to produce C_3H_8 , which is subsequently dehydrogenated to form a $C_3H_7^{\bullet}$ radical. However, the $C_3H_7^{\bullet}$ radical can also be formed through the coupling of C_2H_4 and CH_3^{\bullet} radicals (Steps 31–33 in Table S1). $C_3H_7^{\bullet}$ radicals can undergo only dehydrogenation, to form C_3H_6 (Step 34 in Table S1).

S2. Propagation of reaction entropies

The relationship between model descriptors and kinetic parameters is schematized in Figure 4 of the main manuscript, and the surface reaction entropies calculated from chemisorption entropies are evenly propagated to the initial prefactor estimates in Table S2 by using Eqs. 35 and 36 in the main manuscript.

Table S2. Initial estimates of prefactors used. Prefactor units: molecular adsorptions, $m_g^3 \text{ kmol}^{-1} \text{ s}^{-1}$; molecular desorptions, s^{-1} ; dissociative adsorptions, $m_g^3 m_c^2 \text{ kmol}^{-2} \text{ s}^{-1}$; associative desorptions, $m_c^2 \text{ kmol}^{-1} \text{ s}^{-1}$; Eley–Rideal reactions, $m_g^3 \text{ kmol}^{-1} \text{ s}^{-1}$; Langmuir–Hinshelwood steps, $m_c^2 \text{ kmol}^{-1} \text{ s}^{-1}$.

Step	Equation	Initial A_j^f	Initial A_j^b
1	$\text{O}_2(\text{g}) + 2^*(\text{s}) \rightleftharpoons 2\text{O}^*(\text{s})$	$1 \cdot 10^{18}$	$2 \cdot 10^{20}$
2	$\text{H}_2\text{O}(\text{g}) + ^*(\text{s}) \rightleftharpoons \text{H}_2\text{O}^*(\text{s})$	$2 \cdot 10^9$	$2 \cdot 10^{13}$
3	$\text{CO}_2(\text{g}) + ^*(\text{s}) \rightleftharpoons \text{CO}_2^*(\text{s})$	$3 \cdot 10^8$	$2 \cdot 10^{13}$
4	$\text{CO}(\text{g}) + ^*(\text{s}) \rightleftharpoons \text{CO}^*(\text{s})$	$1 \cdot 10^6$	$2 \cdot 10^{13}$
5	$\text{CH}_4(\text{g}) + \text{O}^*(\text{s}) \rightleftharpoons \text{CH}_3^*(\text{g}) + \text{OH}^*(\text{s})$	$3 \cdot 10^{10}$	$3 \cdot 10^{10}$
6	$\text{C}_2\text{H}_6(\text{g}) + \text{O}^*(\text{s}) \rightleftharpoons \text{C}_2\text{H}_5^*(\text{g}) + \text{OH}^*(\text{s})$	$2 \cdot 10^{10}$	$2 \cdot 10^{10}$
7	$\text{C}_2\text{H}_5^*(\text{g}) + \text{O}^*(\text{s}) \rightleftharpoons \text{C}_2\text{H}_4(\text{g}) + \text{OH}^*(\text{s})$	$2 \cdot 10^{10}$	$2 \cdot 10^{10}$
8	$\text{C}_2\text{H}_4(\text{g}) + \text{O}^*(\text{s}) \rightleftharpoons \text{C}_2\text{H}_3^*(\text{g}) + \text{OH}^*(\text{s})$	$2 \cdot 10^{10}$	$2 \cdot 10^{10}$
9	$\text{CH}_3^*(\text{g}) + \text{O}^*(\text{s}) \rightleftharpoons \text{CH}_3\text{O}^*(\text{s})$	$2 \cdot 10^7$	$2 \cdot 10^{13}$
10	$\text{CH}_3\text{O}^*(\text{s}) + \text{O}^*(\text{s}) \rightleftharpoons \text{CH}_2\text{O}^*(\text{s}) + \text{OH}^*(\text{s})$	$1 \cdot 10^{18}$	$1 \cdot 10^{18}$
11	$\text{CH}_3\text{O}^*(\text{g}) + \text{O}^*(\text{s}) \rightleftharpoons \text{CH}_2\text{O}^*(\text{g}) + \text{OH}^*(\text{s})$	$2 \cdot 10^{10}$	$2 \cdot 10^{10}$
12	$\text{C}_2\text{H}_4(\text{g}) + \text{O}^*(\text{s}) \rightleftharpoons \text{CH}_3\text{CHO}^*(\text{s})$	$1 \cdot 10^6$	$2 \cdot 10^{13}$
13	$\text{CH}_3\text{CHO}^*(\text{s}) + \text{O}^*(\text{s}) \rightleftharpoons \text{CH}_2\text{CHO}^*(\text{s}) + \text{OH}^*(\text{s})$	$1 \cdot 10^{19}$	$1 \cdot 10^{19}$
14	$\text{CH}_2\text{CHO}^*(\text{s}) + \text{O}^*(\text{s}) \rightleftharpoons \text{CH}_2\text{O}^*(\text{s}) + \text{CHO}^*(\text{s})$	$1 \cdot 10^{19}$	$1 \cdot 10^{18}$
15	$\text{CH}_2\text{O}^*(\text{s}) + \text{O}^*(\text{s}) \rightleftharpoons \text{CHO}^*(\text{s}) + \text{OH}^*(\text{s})$	$1 \cdot 10^{18}$	$1 \cdot 10^{18}$
16	$\text{CH}_2\text{O}^*(\text{g}) + \text{O}^*(\text{s}) \rightleftharpoons \text{CHO}^*(\text{g}) + \text{OH}^*(\text{s})$	$2 \cdot 10^{10}$	$2 \cdot 10^{10}$
17	$\text{CHO}^*(\text{s}) + \text{O}^*(\text{s}) \rightleftharpoons \text{CO}^*(\text{s}) + \text{OH}^*(\text{s})$	$1 \cdot 10^{18}$	$1 \cdot 10^{18}$
18	$\text{CHO}^*(\text{g}) + \text{O}^*(\text{s}) \rightleftharpoons \text{CO}(\text{g}) + \text{OH}^*(\text{s})$	$2 \cdot 10^{10}$	$2 \cdot 10^{10}$
19	$\text{CO}^*(\text{s}) + \text{O}^*(\text{s}) \rightleftharpoons \text{CO}_2^*(\text{s}) + ^*(\text{s})$	$1 \cdot 10^{18}$	$1 \cdot 10^{18}$
20	$\text{H}_2(\text{g}) + \text{O}^*(\text{s}) \rightleftharpoons \text{H}^*(\text{g}) + \text{OH}^*(\text{s})$	$1 \cdot 10^{11}$	$1 \cdot 10^{11}$
21	$\text{H}_2\text{O}(\text{g}) + \text{O}^*(\text{s}) \rightleftharpoons \text{OH}^*(\text{g}) + \text{OH}^*(\text{s})$	$3 \cdot 10^{10}$	$3 \cdot 10^{10}$
22	$\text{OH}^*(\text{g}) + \text{O}^*(\text{s}) \rightleftharpoons \text{O}^*(\text{g}) + \text{OH}^*(\text{s})$	$3 \cdot 10^{10}$	$3 \cdot 10^{10}$
23	$\text{H}_2\text{O}_2(\text{g}) + \text{O}^*(\text{s}) \rightleftharpoons \text{HO}_2^*(\text{g}) + \text{OH}^*(\text{s})$	$2 \cdot 10^{10}$	$2 \cdot 10^{10}$
24	$\text{HO}_2^*(\text{g}) + \text{O}^*(\text{s}) \rightleftharpoons \text{O}_2(\text{g}) + \text{OH}^*(\text{s})$	$2 \cdot 10^{10}$	$2 \cdot 10^{10}$
25	$\text{HO}_2^*(\text{g}) + ^*(\text{s}) \rightleftharpoons \text{OH}^*(\text{g}) + \text{O}^*(\text{s})$	$2 \cdot 10^{10}$	$3 \cdot 10^{10}$
26	$\text{OH}^*(\text{s}) + \text{OH}^*(\text{s}) \rightleftharpoons \text{H}_2\text{O}^*(\text{s}) + \text{O}^*(\text{s})$	$2 \cdot 10^{18}$	$2 \cdot 10^{18}$

Forward adsorption step prefactors correspond to an initial sticking coefficient guess of 0.2 (O_2), 0.05 (H_2O), 0.01 (CO_2), 10^{-4} (CH_3^\bullet), 10^{-5} (CO), and 10^{-5} (C_2H_4), following the hierarchical order of magnitude of the results reported by Kechagiopoulos et al.²⁰ Orders of magnitude of desorption prefactors have been taken from Dumesic et al.³³ by assuming similar freedom, and thus, a ratio partition function close to unity for the adsorbed intermediate and its preceding transition state for molecular desorptions and immobile adsorbed and transition states for the associative desorption of O_2 . For Eley–Rideal steps, the reference used in this work was the comparison of the reactant mobility with that of the transition state reported by Sun et al.,²⁰ which is similar to the estimates of Dumesic et al.³³ under the assumption of an immobile transition state and those of Su et al.³⁴ Additional mobility was granted to the transition state of the H-abstraction step from H_2 . For all Langmuir–Hinshelwood reactions, transition state rotation was included in the mobility assessment for the consideration of the prefactor estimates.

S3. Orthogonal collocation and number of collocation points

The system of equations defined by the continuity equations for both phases is a set of partial differential-algebraic equations (PDEs), with $2 N_{s,g}$ differential equations (one for each continuity equation and gas-phase species) from Eqs. 3 and 4 in the main manuscript and $N_{s,s} + 1$ algebraic equations from Eqs. 8 and 9 for the surface intermediates and vacancies, respectively. In order to simplify the mathematical solution of this problem, the orthogonal collocation (OC) method is proposed. This method is a powerful numerical technique used for solving differential equation problems, and it involves the discretization of a given spatial domain by representing the unknown solution in that domain as a series expansion of well-defined functions, often polynomials, referred to as trial functions. By fitting the coefficients of these trial functions at specific grid points, known as collocation points, the solution can be accurately approximated. A key aspect of the OC method is ensuring that the solution satisfies the governing equations at these collocation points, leading to a residual of zero. The choice of the trial function shape depends on the nature of the problem being solved. In the case of symmetric problems (applicable to both interstitial and intraparticle phases), the trial function can be conveniently expressed as a summation of polynomials with even powers. This symmetry property of the trial function reduces the number of unknown coefficients by a factor of 2, making the solution process more efficient.³⁵ For a symmetrical problem, the trial function can be written as

$$y^*(x^2) = b + (1 - x^2) \sum_{i=1}^{N_c} (a_i P_i(x^2)) \quad (S1)$$

where y^* is the trial function that approximates the true solution, x represents the vector of collocation points or mesh of the coordinate being discretized, a_i and b are the coefficients of the trial polynomial that adjust the trial function to fit the given problem, N_c is the number of collocation points excluding the boundary points, and P is the orthogonal polynomial whose N_c roots are the collocation points, thus satisfying the differential equation at those points.

To summarize, the trial function y^* is constructed using orthogonal polynomials and fitted using coefficients a_i and b at the collocation points x that are part of the discretized domain. The objective is to determine the optimal coefficients that minimize the residual error and provide a good approximation of the true solution. The optimal coefficients are obtained through the following steps.

1. Within the set of equations to be solved, define the spatial domain that can be discretized.
2. Discretize the spatial domain through the determination of the collocation points by finding the roots of the orthogonal polynomial.
3. Approximate and evaluate the original equations by using trial functions at the collocation points.
4. Solve the resulting system of simplified equations.

The continuity equations discussed in this study involve two primary spatial domains: the radial coordinates of the interstitial and intraparticle phases (r and ξ , respectively), and the axial coordinate of the reactor (z). To handle these equations effectively, the radial coordinates should be discretized while maintaining the axial coordinate continuous. In this manner, the continuity equation of the interstitial phase is transformed into a system of ordinary differential equations (ODEs), while the continuity equation of the intraparticle phase becomes a set of algebraic equations. Thus, the problem can be considered as a standard set of differential-algebraic equations (DAEs).

In OC, the discretization of the spatial domain proceeds through the determination of the collocation points. Various methods and criteria exist for determining collocation points. In this study, the procedure described by Finlayson^{35,36} was followed; it is known to produce accurate results. For symmetrical problems, the approach involves finding the roots of an orthogonal polynomial of even powers up to $2N_c$, where N_c represents the number of interior collocation points excluding the boundary point. When the orthogonal polynomial is defined, setting the first coefficient to 1 accounts for the trivial contribution of the boundary point, and therefore, the remaining N_c coefficients of the following polynomial should be determined:

$$P(x^2) = 1 + \sum_{i=1}^{N_c} \kappa_i x_j^{2i} \quad (\text{S2})$$

In order to make the previous polynomial valid for OC, through the following orthogonality constraint, the coefficients of the polynomial (κ_i in Eq. S2) whose roots are the collocation points can be obtained:

$$\int_0^1 w(x^2) P(x^2) x^{2i} x^{a-1} dx = 0 \quad i = 1, \dots, N_c \quad (\text{S3})$$

where $w(x^2)$ is the weight function, $P(x^2)$ is the proposed polynomial, and a is the geometry factor of the problem. For interstitial and intraparticle phases, that is, for cylindrical and spherical geometries respectively, values of a are 2 and 3. By applying these conditions, we can compute the coefficients of the N_c^{th} order Jacobi polynomial, and its roots are considered as the collocation points. This procedure can be used for any number of interior points (N_c) and any geometry (a value). Finally, the boundary collocation point ($x_{N_c+1} = 1$) is appended by default.³⁷ The purpose of the weight function is to assign different weights or importance to different points within the integration interval, and common choices include weights derived from quadrature formulas (e.g., the Radau quadrature where $w = 1 - x^2$).

Once the collocation points have been determined, the next step is to approximate and evaluate the original equations using the trial functions. For this step, the trial function is formulated using the collocation points. In the case of symmetrical problems, a symmetrical nodal polynomial is proposed as the trial function at the j^{th} collocation point:

$$y_j^* = \sum_{i=1}^{N_c+1} (d_i x_j^{2i-2}) \quad j = 1, \dots, N_c + 1 \quad (\text{S4})$$

where y_j^* is the trial function at a specific collocation point x_j and d_i is the i^{th} term of the trial function of the coefficient vector, determined from the solution of the collocation problem. Vector d essentially contains a and b terms in Eq. S1. Eq. S4 can be generalized to include all collocation points in a matrix form as follows:

$$y^* = \begin{bmatrix} y_1^* \\ \vdots \\ y_{N_c+1}^* \end{bmatrix} = \begin{bmatrix} 1 & x_1^2 & \cdots & x_1^{2N_c} \\ \vdots & \vdots & \ddots & \vdots \\ 1 & x_{N_c+1}^2 & \cdots & x_{N_c+1}^{2N_c} \end{bmatrix} \cdot \begin{bmatrix} d_1 \\ \vdots \\ d_{N_c+1} \end{bmatrix} = Q \cdot d \quad (\text{S5})$$

where Q ($Q \in \mathbb{R}^{N_c+1 \times N_c+1}$) represents the collocation matrix and d ($d \in \mathbb{R}^{N_c+1}$) represents the coefficients of the trial functions. Each entry of the matrix Q corresponds to the value of a collocation point raised to an even power, as Q is the term of the collocation point in Eq. S4. Since the shape of the solution is known (Eq. S4), the first derivative of the trial function at the j^{th} collocation point, and hence the expected solution, can be obtained as

$$\frac{dy_j^*}{dx} = \frac{d}{dx} \left(\sum_{i=1}^{N_c+1} (d_i x_j^{2i-2}) \right) = \sum_{i=1}^{N_c+1} \left(d_i \frac{dx_j^{2i-2}}{dx} \right) \quad j = 1, \dots, N_c + 1 \quad (\text{S6})$$

which in the generalized matrix form for the entire collocation point grid becomes essentially the matrix product of the derivative of Q and d :

$$\frac{dy^*}{dx} = \begin{bmatrix} 0 & 1 & \cdots & 2N_c \cdot x_1^{2N_c-1} \\ \vdots & \vdots & \ddots & \vdots \\ 0 & 1 & \cdots & 2N_c \cdot x_{N_c+1}^{2N_c-1} \end{bmatrix} \cdot \begin{bmatrix} d_1 \\ \vdots \\ d_{N_c+1} \end{bmatrix} = C \cdot d \quad (\text{S7})$$

where C ($C \in \mathbb{R}^{N_c+1 \times N_c+1}$) is the derivative of the collocation matrix. Since isolating d from Eq. S5 yields $d = Q^{-1} y^*$, the first derivative of y^* in Eq. S8 can be written as a function of the trial function itself:

$$\frac{dy^*}{dx} = C \cdot d = (C \cdot Q^{-1}) \cdot y^* = A \cdot y^* \quad (\text{S8})$$

Eq. S8 reflects the fundamental idea of OC, as it allows differential operators to be expressed in terms of the trial function, thereby transforming the system's complexity from the differential level to the algebraic level. Notably, in Eq. S8, the matrix A can be computed in advance, as it depends only on the collocation points chosen for discretization. Similarly, the Laplacian of the trial function at the j^{th} collocation point can be computed analogously:

$$\nabla^2 y_j^* = \nabla^2 \left(\sum_{i=1}^{N_c+1} (d_i x_j^{2i-2}) \right) = \sum_{i=1}^{N_c+1} (d_i \nabla^2 (x_j^{2i-2})) \quad (\text{S9})$$

On the basis of the trial function for the entire grid, the Laplacian is given by

$$\nabla^2 y^* = D \cdot d = (D \cdot Q^{-1}) \cdot y^* = (C \cdot V \cdot T \cdot Q^{-1}) \cdot y^* = B \cdot y^* \quad (\text{S10})$$

where D ($D \in \mathbb{R}^{N_c+1 \times N_c+1}$) is the characteristic Laplacian matrix, C is the derivative of the collocation matrix in Eq. S7, V ($V \in \mathbb{R}^{N_c+1 \times N_c+1}$) is the collocation-point-independent matrix of D , and T ($T \in \mathbb{R}^{N_c+1 \times N_c+1}$) is the geometry-independent matrix of D . The decomposition of D yields C , V , and T in Eq. S10. Note that the computation of the Laplacian is geometry sensitive (V is geometry dependent) because the choice of discretization strategy and the arrangement of collocation points depend on the geometry of the system, and these factors directly affect the accuracy and reliability of the Laplacian computation. C , V , and T for different geometries are provided in Table S3.

Table S3. V and T matrices for the geometries of interest.

	V	T
Cylindrical geometry	$\begin{bmatrix} 0 & 2 & 4 & \cdots & 2N_c \\ \vdots & \vdots & \vdots & \ddots & \vdots \\ 0 & 2 & 4 & \cdots & 2N_c \end{bmatrix}$	$\begin{bmatrix} 0 & 1 & x_1^2 & \cdots & x_1^{2N_c-2} \\ \vdots & \vdots & \vdots & \ddots & \vdots \\ 0 & 1 & x_{N_c+1}^2 & \cdots & x_{N_c+1}^{2N_c-2} \end{bmatrix}$
Spherical geometry	$\begin{bmatrix} 0 & 3 & 5 & \cdots & 2N_c+1 \\ \vdots & \vdots & \vdots & \ddots & \vdots \\ 0 & 3 & 5 & \cdots & 2N_c+1 \end{bmatrix}$	

Matrix D can be decomposed into matrices C , V , and T by calculating the Laplacian of the trial function at the j^{th} collocation point for both cylindrical (interstitial phase) and spherical (intraparticle phase) systems as

$$\nabla^2 y_j^* = \frac{1}{r_j} \frac{d}{dr} \left(r_j \frac{dy_j^*}{dr} \right) = \frac{1}{r_j} \frac{d}{dr} \left(r_j \sum_{i=1}^{N_c+1} \left(d_i \frac{dr_j^{2i-2}}{dr} \right) \right) \quad (\text{S11})$$

$$\nabla^2 y_j^* = \frac{1}{\xi_j^2} \frac{d}{d\xi} \left(\xi_j^2 \frac{dy_j^*}{d\xi} \right) = \frac{1}{\xi_j^2} \frac{d}{d\xi} \left(\xi_j^2 \sum_{i=1}^{N_c+1} \left(d_i \frac{d\xi_j^{2i-2}}{d\xi} \right) \right) \quad (\text{S12})$$

The number of collocation points can also affect the computation of the coefficients required for obtaining the results, as the inversion of matrix Q should be performed. Inversion of Q can be done reliably for $N_c < 10$, with a loss of a few digits. However, as N_c is increased, A and B (from Eqs. S8 and S10) are poorly matched with the collocation abscissae, as Q becomes nearly singular. In such cases, other methods, such as the one proposed by Michelsen and Villadsen,³⁸ are required. To ease the task of matrix inversion, we express the radial coordinates of the interstitial and intraparticle phases in their dimensionless form in the continuity equations.

After the differential operators are approximated using the trial functions, the set of $2 N_{s,g}$ differential equations, one per continuity equation and gas-phase species ($N_{s,g}$), is effectively simplified. From every partial differential equation for each gas-phase species in the interstitial phase, a set of $N_{c,g}$ ODEs (with respect to z) is obtained, where $N_{c,g}$ denotes the number of interior collocation points chosen for the radial discretization of the interstitial phase. The intraparticle phase continuity equation for each gas-phase species can be reduced to a set of $N_{c,s}$ algebraic equations for being ξ dependent exclusively, where $N_{c,s}$ denotes the number of interior collocation points chosen for the radial discretization of the intraparticle phase. The number of collocation points used in each phase may differ. Furthermore, enforcing the boundary conditions at both phases leads to the inclusion of two additional algebraic equations per gas-phase species. This arises from the concentration equality (Eq. 6 in the main manuscript) and the derivatives in the mass flux conservation (Eq. 4 in the main manuscript) being expressed as functions of the trial function. Moreover, selecting a symmetrical function for the trial function, specifically a polynomial of even powers, automatically enforces the symmetry boundary conditions for the concentration with respect to the radial coordinate at $r = 0$ or $\xi = 0$ in each phase (Eqs. 3 and 5). The pseudo-steady-state approximation across the intraparticle phase introduces additional $N_{c,s}$ algebraic equations per surface-intermediate ($N_{s,s}$) as it is to be

evaluated at the interior points and at $\xi = 1$. The site balance (Eq. 9 in the main manuscript) contributes $N_{c,s}$ more algebraic equations. The contribution of each term is detailed in Table S4.

Table S4. Contribution of model terms to total number of equations. Gas and surface denote gas-phase species and surface intermediates, totaling $N_{s,g}$ and $N_{s,s}$ number of species, respectively. $N_{c,g}$ and $N_{c,s}$ denote the number of collocation points in the interstitial and intraparticle phases, respectively.

Term	No. of differential equations	No. of algebraic equations
Interstitial phase (gas)		
Continuity	$N_{c,g} \cdot N_{s,g}$	–
Left boundary	–	0 (because of even-powered trial function)
Right boundary	–	$N_{s,g}$
Intraparticle phase (gas)		
Continuity	–	$N_{c,s} \cdot N_{s,g}$
Left boundary	–	0 (because of even-powered trial function)
Right boundary	–	$N_{s,g}$
Intraparticle phase (surface)		
Pseudo-steady-state approximation	–	$(N_{c,s} + 1) \cdot N_{s,s}$
Active site balance	–	$(N_{c,s} + 1)$
Total number of equations	$N_{c,g} \cdot N_{s,g}$	$2 N_{s,g} + N_{s,s} + 1 + (N_{s,g} + N_{s,s} + 1) \cdot N_{c,s}$

Table S4 clarifies the direct correlation between the number of differential equations within the system and the collocation points in the interstitial phase ($N_{c,g}$). This correlation is delineated by a proportionality constant contingent upon the number of gaseous species. Furthermore, the number of algebraic equations increases in direct proportion to both the cumulative species count in the gaseous and surface phases ($N_{s,g} + N_{s,s}$) and the augmentation of collocation points in the intraparticle phase ($N_{c,s}$). It is imperative to underscore that the species count in each phase is intrinsically determined by the intricacy of the reaction network. This necessitates the meticulous determination of the appropriate collocation points to ensure accurate solutions while concurrently reducing computational expenses. Consequently, neither should be arbitrarily defined; this is one of the main benefits of using Chen et al.'s model¹⁵ for accounting for the homogeneous reaction mechanism.

Before embarking on parameter estimation for the 1D heterogeneous reactor, we should determine the number of collocation points to be used. For this, an extensive parameter search is conducted using a PFR and a genetic algorithm, which is computationally more feasible than the use of a 1D heterogeneous reactor model. The parameters estimated from this search are used to investigate the effect of the number of collocation points on the computation of the 1D heterogeneous reactor (Figure S1).

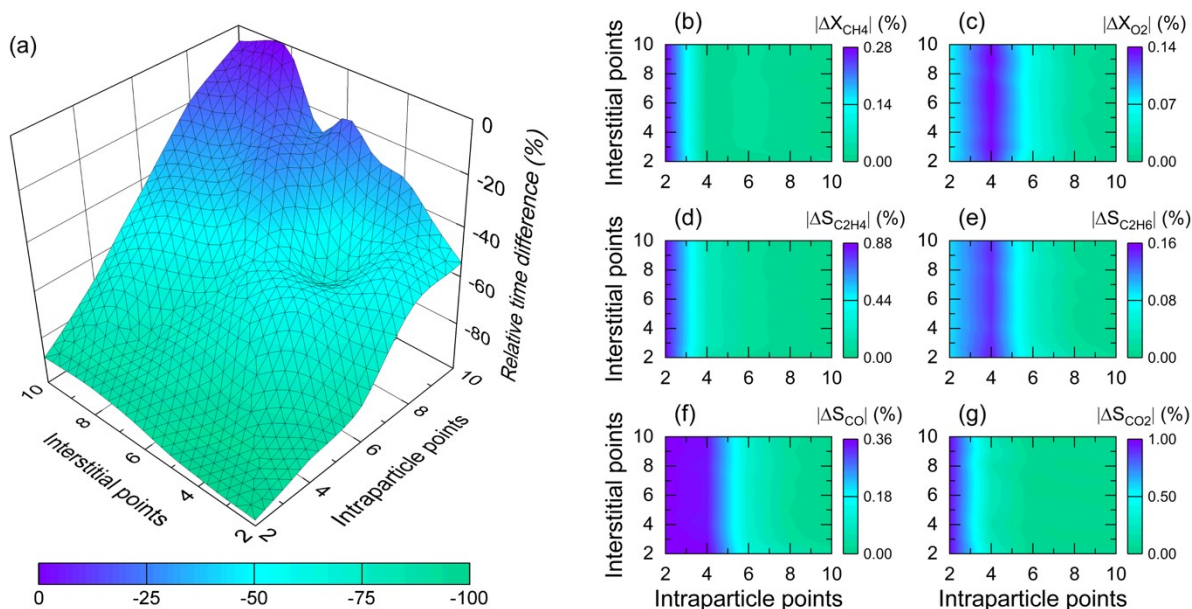


Figure S1. Effect of number of collocation points of both interstitial and intraparticle phases on (a) the computation time required for integration of the 1D heterogeneous reactor, expressed as a relative difference with respect to the highest recorded value. (b–g) Absolute difference of simulated performance metrics with respect to the case with the maximum number of collocation points in both phases (i.e., 10 for each phase). Simulation conditions: IMP SiO₂ catalyst with descriptors from the genetic algorithm employing a plug-flow reactor model, $T = 800$ °C, $P = 1$ bar, feed molar ratio of CH₄/O₂/He = 3/1/0.6, $W/F_{\text{CH}_4,0} = 3.0$ g_c h mol_C⁻¹ from the equivalent $L = 0.02$ m.

The objective of this study was to establish a balance between computational efficiency and model accuracy, a consideration intricately linked to the complexity of the task of solving the associated system of DAEs. As evidenced in Figure S1a, an increase in collocation points, especially the number of collocation points in the intraparticle phase, correlates proportionally with an increase in the computation time. This observation is not unexpected, since the intraparticle phase contributes 35 algebraic equations per interior

collocation point (excluding an additional 35 from boundary conditions). This contrasts with the 24 differential equations contributed by the interstitial phase per interior collocation point (excluding an additional 24 from boundary conditions). In fact, a discernible reduction in computational time by over 80% is achievable when the number of intraparticle collocation points is decreased from ten to three, and even at a considerable number of interstitial collocation points. Such an effect becomes less pronounced as the number of interstitial collocation points decreases. This relationship stresses the interplay between spatial discretization, represented by collocation points, and the numerical complexity inherent in solving the model equations.

An analysis of reactant conversions (Figures S1b,c) across various cases shows nuanced variations, underscoring the direct effect of collocation points on the evolution of gas-phase species within the reactor. For these metrics, the number of interstitial points does not appear to influence the estimated conversion significantly, unlike intraparticle collocation points. Furthermore, on the basis of conversions, the total number of intraparticle collocation points can be considered sufficient when set at seven. An examination of product selectivity (Figures S1d–g) further accentuates the role of spatial discretization. Changes in intraparticle collocation points affect not only the overall conversion but also the distribution of products. In fact, for the latter, the effect of the interstitial phase collocation points appears to be more prominent. In any case, seven intraparticle collocation points appear to be sufficient on the basis of product selectivities too, with the effect of the number of interstitial collocation points becoming somewhat irrelevant.

In conclusion, on the basis of observed trends, the number of collocation points can be set at seven and four for the intraparticle and interstitial phases, respectively. This choice serves as a guide for the selection of an appropriate configuration for subsequent time-consuming optimization runs. However, this is not a generalized conclusion, as both computational time and accuracy depend on simulation conditions and the specific kinetic parameters employed.

S4. Temperature-programmed experiments and simulations

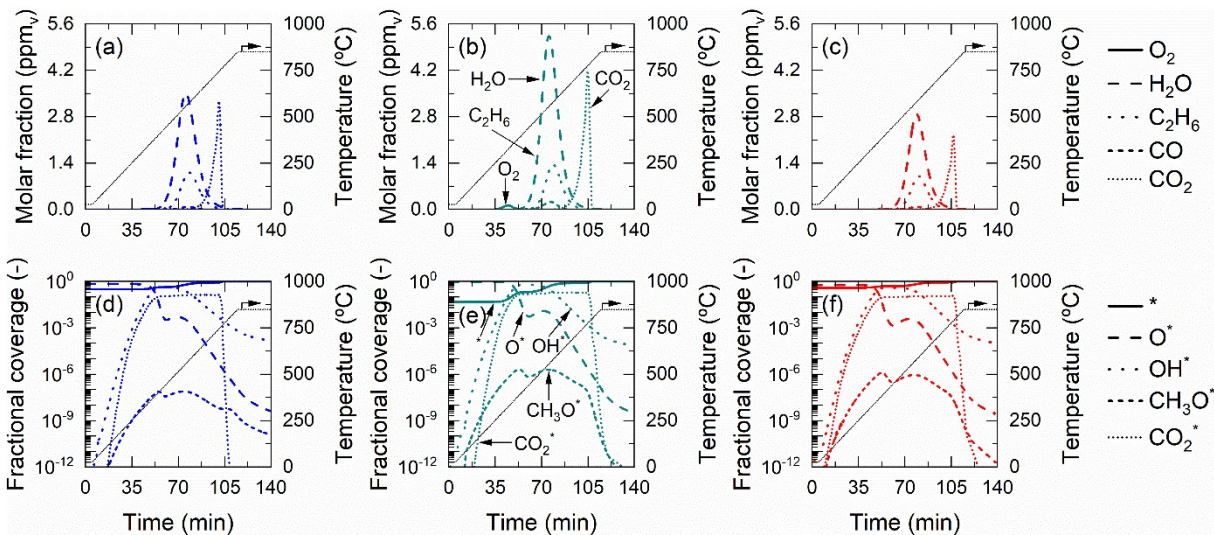


Figure S2. Evolution of predicted temperature-programmed surface reaction of the (a–c) main products and (d–f) main surface intermediates for IMP SiO₂, SD SiO₂-α+βSiC, and SD SiO₂-βSiC. Simulation conditions: $P = 1$ bar, $T_1 = 25$ °C, $T_F = 850$ °C, $\beta = 7.5$ °C min⁻¹, $t_\infty = 30$ min, $F_T = 100$ NmL min⁻¹, $p_{\text{CH}_4,0} = 1$ bar, $W = 50$ mg_c. Simulations were performed assuming plug-flow conditions and by using the model descriptors in Table 5 in the main manuscript.

S5. Regression assessment

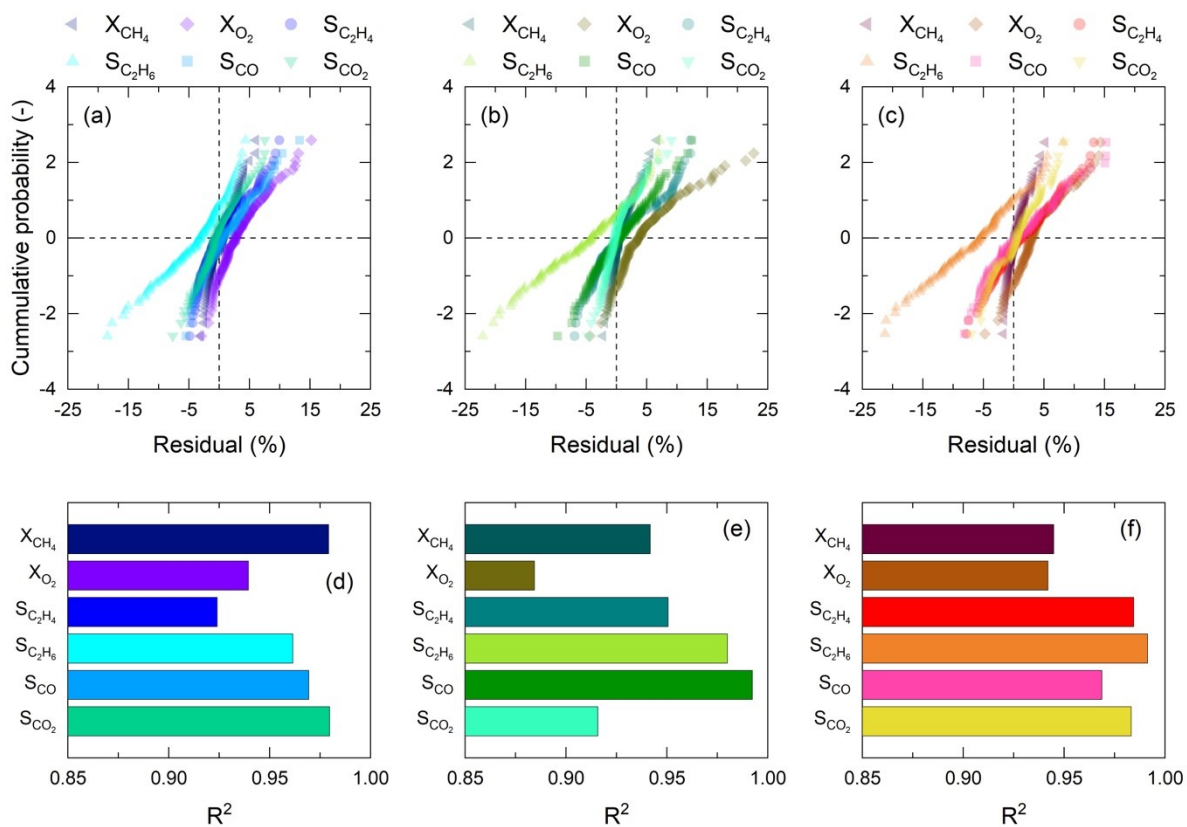


Figure S3. Residual probability plots of the measured and predicted performance metrics for (a) IMP SiO₂, (b) SD SiO₂-α+βSiC, and (c) SD SiO₂-βSiC. The square of the Pearson product moment correlation coefficient for (d) IMP SiO₂, (e) SD SiO₂-α+βSiC, and (f) SD SiO₂-βSiC is also shown.

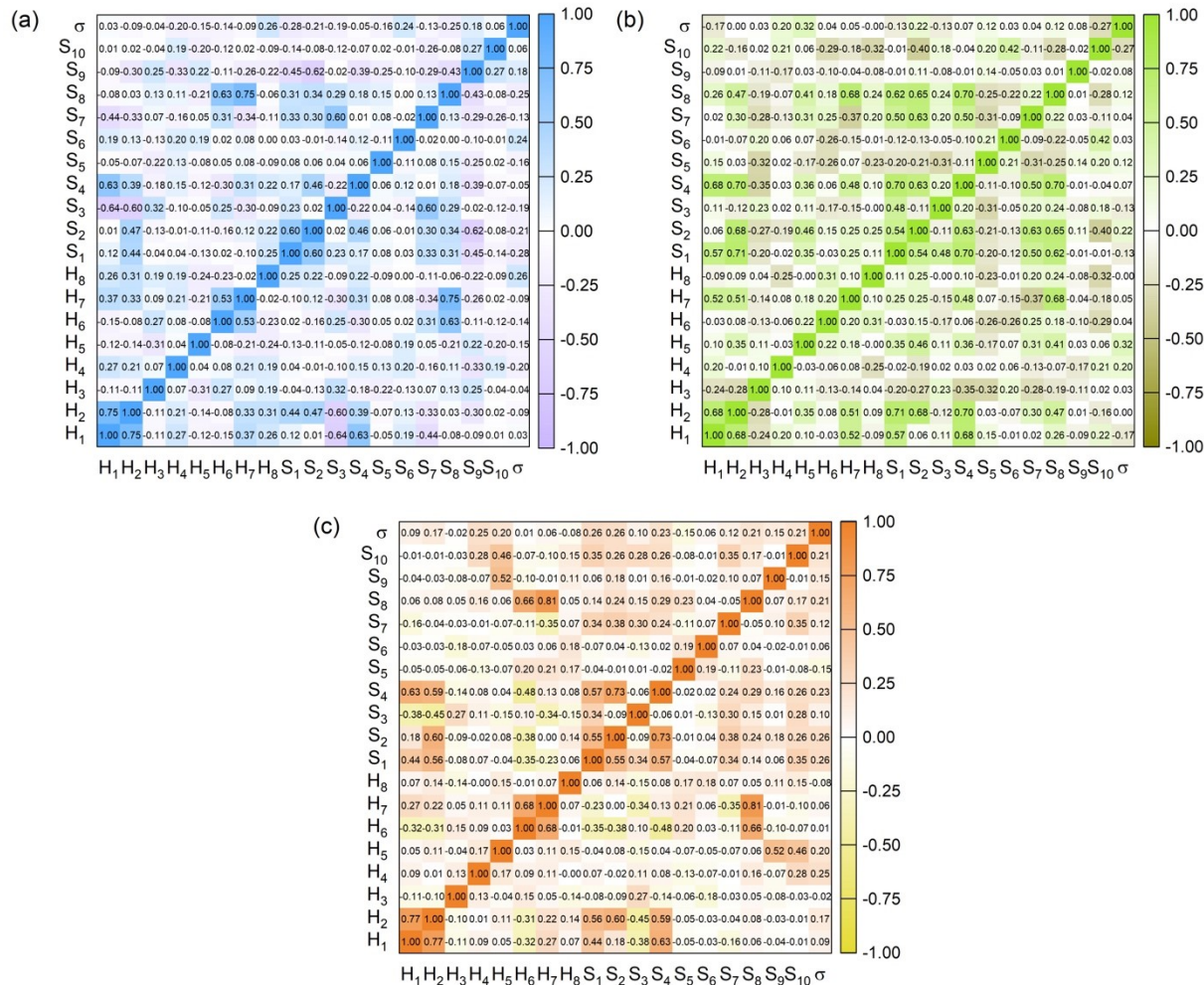


Figure S4. Binary correlation matrix of the descriptors obtained with the microkinetic model in Table 7 in the main manuscript for all three catalysts: (a) IMP SiO₂, (b) SD SiO₂-α+βSiC, and (c) SD SiO₂-βSiC.

S6. Model descriptor benchmarking

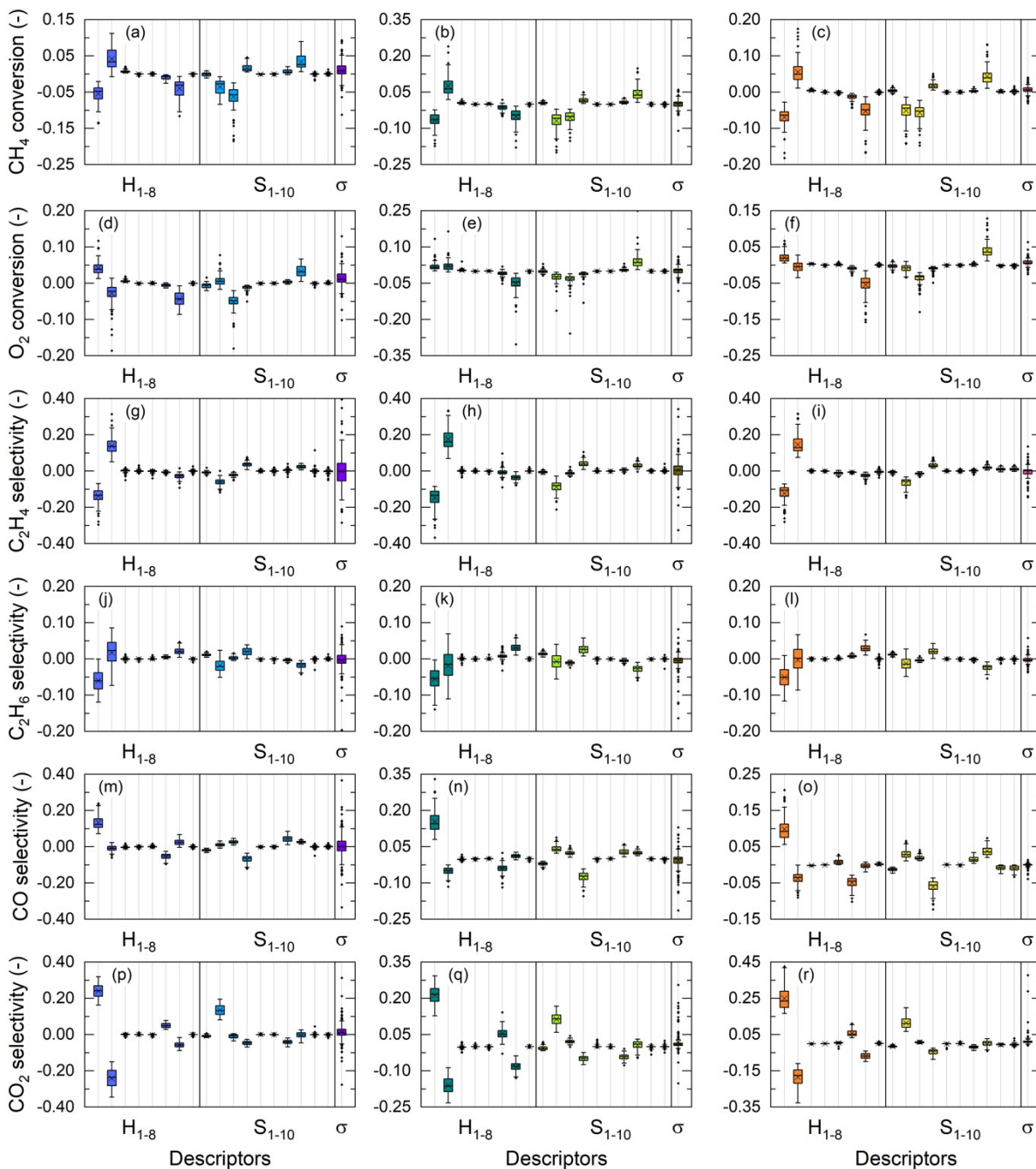


Figure S5. Box plots of the normalized sensitivity coefficients of descriptors obtained with the microkinetic model in Table 7 in the main manuscript with respect to each performance metric over all the experimental conditions: (a–c) CH₄ conversion, (d–f) O₂ conversion, (g–i) C₂H₄ selectivity, (j–l) C₂H₆ selectivity, (m–o) CO selectivity, and (p–r) CO₂ selectivity for IMP SiO₂, SD SiO₂- α + β SiC, and SD SiO₂- β SiC. The cross denotes mean value.

S7. Simulation results

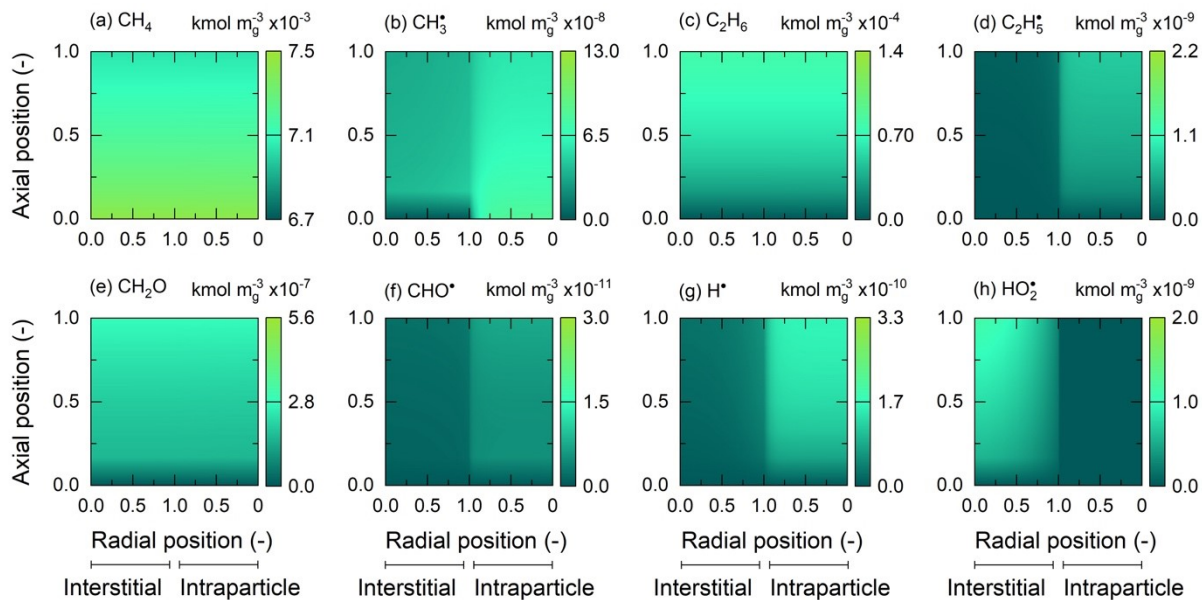


Figure S6. Axial and radial (interstitial and intraparticle phases) concentration profile predictions for SD $\text{SiO}_{2-\alpha+\beta}\text{SiC}$ for (a) CH_4 , (b) CH_3^* , (c) C_2H_6 , (d) C_2H_5^* , (e) CH_2O , (f) CHO^* , (g) H^* , and (h) HO_2^* . Simulation conditions: $T = 800\text{ }^\circ\text{C}$, $P = 1\text{ bar}$, feed molar ratio of $\text{CH}_4/\text{O}_2/\text{He} = 3/1/0.6$, $W/F_{\text{CH}_4,0} = 4.4\text{ g}_c\text{ h mol}_c^{-1}$ from the equivalent $L_b = 0.018\text{ m}$. Simulation results: 5.3% CH_4 conversion, 10.4% O_2 conversion, 31.4% C_2H_4 selectivity, 40.9% C_2H_6 selectivity, 17.9% CO selectivity, 9.7% CO_2 selectivity.

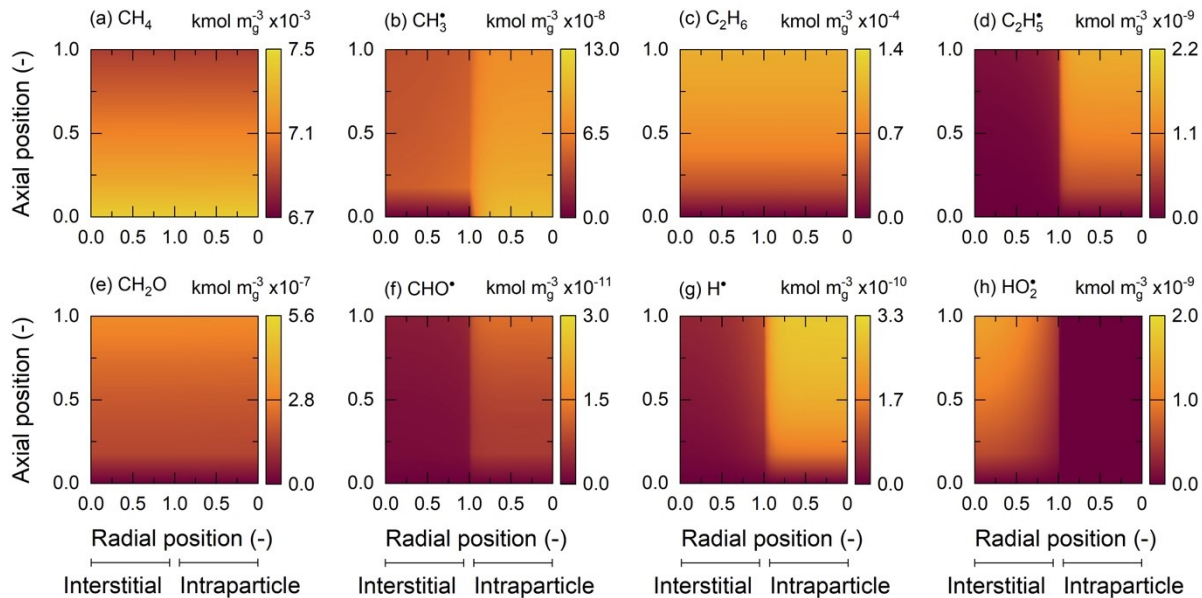


Figure S7. Axial and radial (interstitial and intraparticle phases) concentration profile predictions for SD $\text{SiO}_2\text{-}\beta\text{SiC}$ for (a) CH_4 , (b) CH_3^* , (c) C_2H_6 , (d) C_2H_5^* , (e) CH_2O , (f) CHO^* , (g) H^* , and (h) HO_2^* . Simulation conditions: $T = 800\text{ }^\circ\text{C}$, $P = 1\text{ bar}$, feed molar ratio of $\text{CH}_4/\text{O}_2/\text{He} = 3/1/0.6$, $W/F_{\text{CH}_4,0} = 4.4\text{ g}_c\text{ h mol}_c^{-1}$ from the equivalent $L_b = 0.017\text{ m}$. Simulation results: 7.6% CH_4 conversion, 15.1% O_2 conversion, 33.6% C_2H_4 selectivity, 38.2% C_2H_6 selectivity, 18.1% CO selectivity, 10.1% CO_2 selectivity.

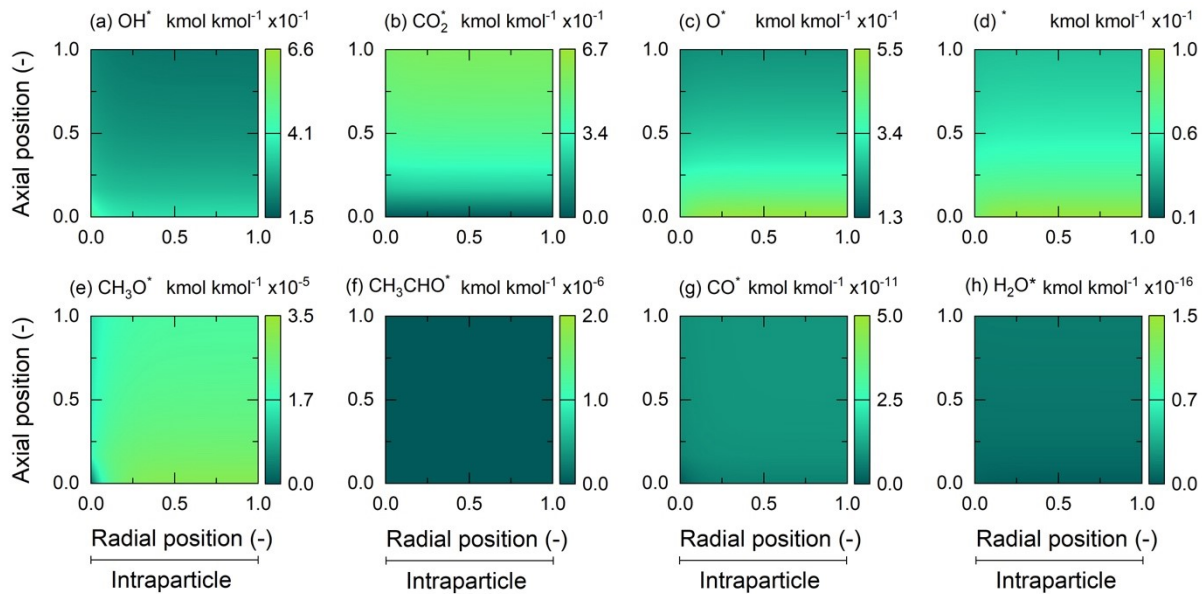


Figure S8. Axial and radial (intraparticle phase) fractional coverage profile predictions for SD SiO₂- $\alpha+\beta$ SiC for (a) OH*, (b) CO₂*, (c) O*, (d) * (vacancies), (e) CH₃O*, (f) CH₃CHO*, (g) CO*, and (h) H₂O*. Simulation conditions and results were identical to those of Figure S6.

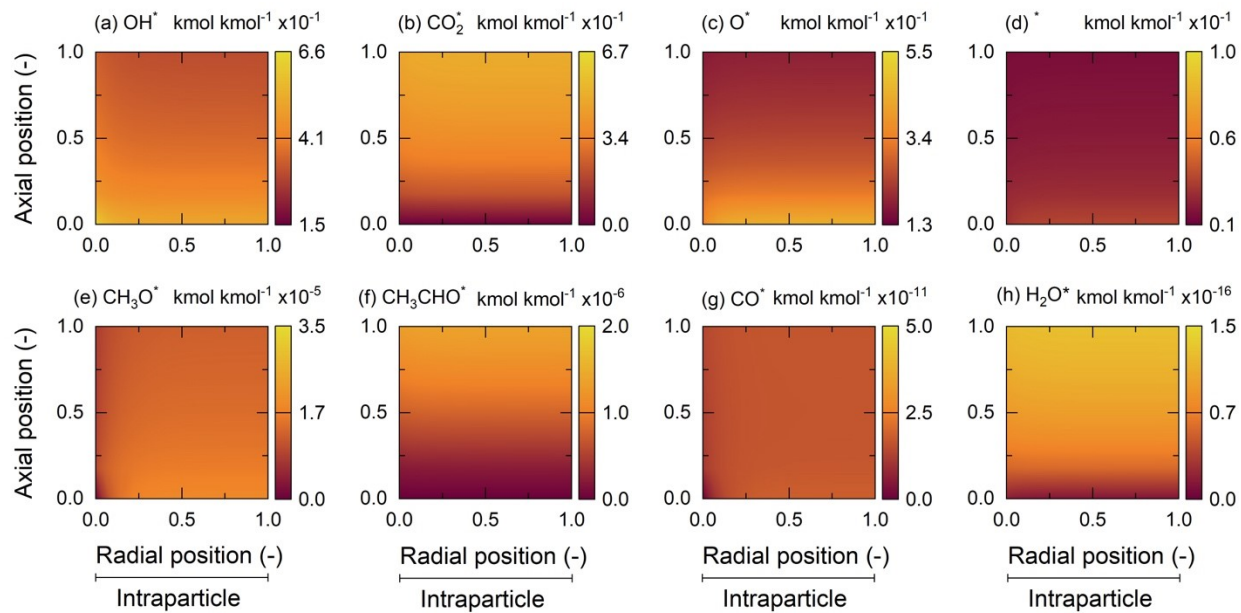


Figure S9. Axial and radial (intraparticle phase) fractional coverage profile predictions for SD SiO₂-βSiC for (a) OH*, (b) CO₂*, (c) O*, (d) * (vacancies), (e) CH₃O*, (f) CH₃CHO*, (g) CO*, and (h) H₂O*. Simulation conditions and results were identical to those of Figure S7.

S8. Nomenclature

Abbreviations

DAEs	Differential-algebraic equations
OC	Orthogonal collocation
OCM	Oxidative coupling of methane
ODEs	Ordinary differential equations
PDEs	Partial differential-algebraic equations
PFR	Plug-flow reactor

Symbols

A	$A \in \mathbb{R}^{N_c+1 \times N_c+1}$ matrix for the calculation of the derivative of y^* from y^* , c.u.
a	Geometry factor. 1, 2, 3 for planar, cylindrical, and spherical geometries, respectively
a_i	i^{th} coefficient of the trial polynomial, c.u.
A_j	Prefactor of homogeneous or heterogeneous reaction step j , c.u.
B	$B \in \mathbb{R}^{N_c+1 \times N_c+1}$ matrix for the calculation of the Laplacian of y^* from y^* , c.u.
b	Coefficient of the trial polynomial, c.u.
C	$C \in \mathbb{R}^{N_c+1 \times N_c+1}$ derivative of the collocation matrix, unitless
D	$D \in \mathbb{R}^{N_c+1 \times N_c+1}$ Laplacian matrix of the collocation matrix, unitless
d	$d \in \mathbb{R}^{N_c+1}$ vector of coefficients for the trial function, c.u.
$E_{a,j}$	Activation energy of homogeneous or heterogeneous reaction step j , kJ mol^{-1}
N_c	Number of collocation points, excluding the boundary points
$N_{c,g}$	Number of interior collocation points for the interstitial phase
$N_{c,s}$	Number of interior collocation points for the intraparticle phase
$N_{s,g}$	Total number of gas-phase species
$N_{s,s}$	Total number of surface intermediates
P	Orthogonal polynomial whose N_c roots are the collocation points, unitless
Q	$Q \in \mathbb{R}^{N_c+1 \times N_c+1}$ collocation matrix, unitless
T	$T \in \mathbb{R}^{N_c+1 \times N_c+1}$ geometry-independent-matrix of D , unitless
V	$V \in \mathbb{R}^{N_c+1 \times N_c+1}$ collocation-point-independent matrix of D , unitless
w	Weight function in the determination of the orthogonal polynomial, unitless
x	Vector of collocation points, unitless
y^*	Trial function which approximates the true solution of y , c.u.
z	Axial reactor bed coordinate, m_b

Greek symbols

κ_i	i^{th} coefficient of the orthogonal polynomial, unitless
ζ	Radial intraparticle coordinate, dimensionless

S9. References

- 1 H. Wang, C. Shao, J. Gascon, K. Takanahe and S. M. Sarathy, *ACS Omega*, 2021, **6**, 33757–33768.
- 2 C. W. Zhou, Y. Li, U. Burke, C. Banyon, K. P. Somers, S. Ding, S. Khan, J. W. Hargis, T. Sikes, O. Mathieu, E. L. Petersen, M. AlAbbad, A. Farooq, Y. Pan, Y. Zhang, Z. Huang, J. Lopez, Z. Loparo, S. S. Vasu and H. J. Curran, *Combust Flame*, 2018, **197**, 423–438.
- 3 G. Bagheri, E. Ranzi, M. Pelucchi, A. Parente, A. Frassoldati and T. Faravelli, *Combust Flame*, 2020, **212**, 142–155.
- 4 M. Baigmohammadi, V. Patel, S. Martinez, S. Panigrahy, A. Ramalingam, U. Burke, K. P. Somers, K. A. Heufer, A. Pekalski and H. J. Curran, *Energy and Fuels*, 2020, **34**, 3755–3771.
- 5 G. P. Smith, D. M. Golden, M. Frenklach, N. W. Moriarty, B. Eiteneer, M. Goldenberg, C. T. Bowman, R. K. Hanson, S. Song, Jr. William C. Gardiner, V. V. Lissianski and Z. Qin, GRI-Mech 3.0, <http://combustion.berkeley.edu/gri-mech/version30/text30.html>, (accessed 16 December 2021).
- 6 H. Wang, X. You, A. V. Joshi, S. G. Davis, A. Laskin, F. Egolfopoulos and C. K. Law, USC Mech Version II. High-Temperature Combustion Reaction Model of H₂/CO/C₁-C₄ Compounds, http://ignis.usc.edu/USC_Mech_II.htm, (accessed 11 January 2022).
- 7 Y. Simon, F. Baronnet and P. M. Marquaire, *Ind Eng Chem Res*, 2007, **46**, 1914–1922.
- 8 M. Fleys, W. Shan, Y. Simon and P. M. Marquaire, *Ind Eng Chem Res*, 2007, **46**, 1063–1068.
- 9 Y. Simon and P. M. Marquaire, *Fuel*, 2021, **297**, 120683.
- 10 P. Barbe, F. Battin-Leclerc and G. Côme, *Journal de Chimie Physique*, 1995, **92**, 1666–1692.
- 11 C. A. Mims, R. Mauti, A. M. Dean and K. D. Rose, *Journal of Physical Chemistry*, 1994, **98**, 13357–13372.
- 12 H. Zanthoff and M. Baerns, *Ind Eng Chem Res*, 1990, **29**, 2–10.
- 13 J. W. M. H. Geerts, Q. Chen, J. M. N. van Kasteren and K. van der Wiele, *Catal Today*, 1990, **6**, 519–526.
- 14 Q. Chen, J. H. B. J. Hoebink and G. B. Marin, *Ind Eng Chem Res*, 1991, **30**, 2088–2097.
- 15 Q. Chen, P. M. Couwenberg and G. B. Marin, *Catal Today*, 1994, **21**, 309–319.
- 16 Q. Chen, P. M. Couwenberg and G. B. Marin, *AIChE Journal*, 1994, **40**, 521–535.
- 17 C. Karakaya, H. Zhu, B. Zohour, S. Senkan and R. J. Kee, *ChemCatChem*, 2017, **9**, 4538–4551.
- 18 C. Karakaya, H. Zhu, C. Loebick, J. G. Weissman and R. J. Kee, *Catal Today*, 2018, **312**, 10–22.
- 19 S. C. Reyes, E. Iglesia and C. P. Kelkar, *Chem Eng Sci*, 1993, **48**, 2643–2661.
- 20 J. Sun, J. W. Thybaut and G. B. Marin, *Catal Today*, 2008, **137**, 90–102.
- 21 A. Obradović, J. W. Thybaut and G. B. Marin, *Chem Eng Technol*, 2016, **39**, 1996–2010.
- 22 P. N. Kechagiopoulos, J. W. Thybaut and G. B. Marin, *Ind Eng Chem Res*, 2014, **53**, 1825–1840.
- 23 J. Sadeghzadeh Ahari, S. Zarrinpashne and M. T. Sadeghi, *Fuel Processing Technology*, 2013, **115**, 79–87.

- 24 V. I. Alexiadis, M. Chaar, A. van Veen, M. Muhler, J. W. Thybaut and G. B. Marin, *Appl Catal B*, 2016, **199**, 252–259.
- 25 V. I. Alexiadis, J. W. Thybaut, P. N. Kechagiopoulos, M. Chaar, A. C. Van Veen, M. Muhler and G. B. Marin, *Appl Catal B*, 2014, **150–151**, 496–505.
- 26 P. M. Couwenberg, Q. Chen and G. B. Marin, *Ind Eng Chem Res*, 1996, **35**, 3999–4011.
- 27 L. Pirro, P. S. F. Mendes, B. D. Vandegehuchte, G. B. Marin and J. W. Thybaut, *React Chem Eng*, 2020, **5**, 584–596.
- 28 L. Pirro, A. Obradović, B. D. Vandegehuchte, G. B. Marin and J. W. Thybaut, *Ind Eng Chem Res*, 2018, **57**, 16295–16307.
- 29 L. Pirro, P. S. F. Mendes, S. Paret, B. D. Vandegehuchte, G. B. Marin and J. W. Thybaut, *Catal Sci Technol*, 2019, **9**, 3109–3125.
- 30 L. A. Vandewalle, K. M. Van Geem, G. B. Marin and R. Bos, *Ind Eng Chem Res*, 2021, **60**, 6538–6553.
- 31 W. K. Metcalfe, S. M. Burke, S. S. Ahmed and H. J. Curran, *Int J Chem Kinet*, 2013, **45**, 638–675.
- 32 J. H. Lunsford, *Angewandte Chemie International Edition in English*, 1995, **34**, 970–980.
- 33 J. A. Dumesic, D. F. Rudd, L. M. Aparicio, J. E. Rekoske and A. A. Treviño, in *The Microkinetics of Heterogeneous Catalysis*, American Chemical Society (ACS), 1st edn., 1993.
- 34 Y. S. Su, J. Y. Ying and W. H. Green, *J Catal*, 2003, **218**, 321–333.
- 35 B. A. Finlayson, *Catalysis Reviews*, 1974, **10**, 69–138.
- 36 B. A. Finlayson, in *The Method of Weighted Residuals and Variational Principles*, Society for Industrial and Applied Mathematics, Philadelphia, PA, 1972, pp. 96–149.
- 37 J. V. Villadsen and W. E. Stewart, *Chem Eng Sci*, 1967, **22**, 1483–1501.
- 38 M. L. Michelsen and J. Villadsen, *The Chemical Engineering Journal*, 1972, **4**, 64–68.